Mon. Not. R. Astron. Soc. **371,** 569–576 (2006) doi:10.1111/j.1365-2966.2006.10667.x

Spinning-down of moving magnetars in the propeller regime

O. D. Toropina,[1⋆] M. M. Romanova[2] and R. V. E. Lovelace[2,3⋆]

[1]*Space Research Institute, Russian Academy of Sciences, Profsoyuznaya 84/32, Moscow 117997, Russia*
[2]*Department of Astronomy, Cornell University, Ithaca, NY 14853-6801, USA*
[3]*Department of Applied and Engineering Physics, Cornell University, Ithaca, NY 14853-6801, USA*

Accepted 2006 June 7. Received 2006 June 7; in original form 2006 March 2

ABSTRACT

We use axisymmetric magnetohydrodynamic simulations to investigate the spinning-down of magnetars rotating in the propeller regime and moving supersonically through the interstellar medium. The simulations indicate that magnetars spin down rapidly due to this interaction, faster than for the case of a non-moving star. From many simulation runs, we have derived approximate scaling laws for the angular momentum loss rate, $\dot{L} \propto -\eta_{\rm m}^{0.3}\mu^{0.6}\rho^{0.8}\mathcal{M}^{-0.4}\Omega_*^{1.5}$, where ρ is the density of the interstellar medium, $\mathcal{M}$ is the Mach number, μ is the star's magnetic moment, Ω_* is its angular velocity and $\eta_{\rm m}$ is the magnetic diffusivity. A magnetar with a surface magnetic field of 10^{13}–10^{15} G is found to spin down to a period $P > 10^5$–10^6 s in $\sim 10^4$–10^5 yr. There is, however, uncertainty about the value of the magnetic diffusivity so that the time-scale may be longer. We discuss this model in respect of soft gamma-ray repeaters (SGRs) and the isolated neutron star candidate RXJ1856.5−3754.

Key words: magnetic fields – MHD – plasmas – shock waves – stars: neutron – pulsars: general.

1 INTRODUCTION

Some neutron stars referred to as 'magnetars' have unusually large magnetic fields, $B \sim 10^{13}$–10^{15} G (Duncan & Thompson 1992; Thompson & Duncan 1995). Possible candidates for magnetars include anomalous X-ray pulsars and soft gamma-ray repeaters (SGRs) (Kulkarni & Frail 1993; Kouveliotou et al. 1994; Hurley et al. 1999). These objects are associated with supernovae remnants and hence are relatively young (Vasist & Gotthelf 1997; Kouveliotou et al. 1998). Only a few candidates for magnetars have been found so far. The estimated birth rate of magnetars is ∼10 per cent of ordinary pulsars (Kulkarni & Frail 1993; Kouveliotou et al. 1994, 1999) so that there might be many more magnetars which are presently invisible. Their 'visibility' depends on a number of factors. One important factor is the rate of the star's spin-down. If magnetars spin down rapidly to very long periods, then one will not detect spin-modulated variability during flares. Consequently, the identification of the variability with a rotating neutron star would be more difficult.

During the pulsar stage of evolution, magnetars spin down much more rapidly than ordinary pulsars. Consequently, they pass through their pulsar stage much faster, in $\sim 10^4$ yr (Thompson & Duncan 1995). When the light cylinder radius becomes larger than the magnetospheric radius $r_{\rm m}$, the relativistic wind is suppressed by the inflowing matter (Shvartsman 1970) and the star enters the propeller regime where the spin-down is due to the interaction of the star's rotating field with the interstellar medium (ISM) (Davidson & Ostriker 1973; Illarionov & Sunyaev 1975). Magnetars with velocities $v > 100$–200 km s^{-1} interact directly with the ISM. That is, the magnetospheric radius is larger than the gravitational capture radius (Harding & Leventhal 1992; Rutledge 2001; Toropina et al. 2001). In the propeller regime, the rapidly rotating magnetosphere interacts strongly with the supersonically inflowing ISM.

The spin-down rate of supersonically moving magnetars in the propeller regime has been estimated earlier, but different authors have obtained rather different results. For example, Rutledge (2001) estimates a spin-down time of $\sim 4 \times 10^9$ yr for a neutron star with a surface magnetic field $B = 10^{15}$ G and velocity $v = 300\,{\rm km\,s^{-1}}$. On the other hand, Mori and Ruderman (2003) estimate that a magnetar spins down to periods greater than 10^4 s within $\sim 5 \times 10^5$ yr. Mori and Ruderman put forward this model as an explanation of the isolated neutron star (INS) candidate RX J1856.5−3754 which does not show variability.

The propeller stage of evolution has been investigated in non-magnetar cases both theoretically (e.g. Illarionov & Sunyaev 1975; Davies, Fabian & Pringle 1979; Davies & Pringle 1981; Lovelace, Romanova & Bisnovatyi-Kogan 1999; Ikhsanov 2002; Rappaport, Fregeau & Spruit 2004) and with MHD simulations (Wang & Robertson 1985; Romanova et al. 2003, 2004, 2005b; Ustyugova et al. 2006). However, only limited theoretical work has been done for magnetar-type propellers, which propagate through the ISM supersonically (Rutledge 2001; Mori & Ruderman 2003). No MHD simulations of this flow regime have been done previously.

This work presents the first numerical simulations of the interaction of supersonic, fast rotating magnetars with the ISM. Earlier, we

⋆E-mail: toropina@iki.rssi.ru (ODT); lovelace@astro.cornell.edu (RVEL)

investigated supersonic propagation of *non-rotating* strongly magnetized stars through the ISM (Toropina et al. 2001). The present simulations are analogous to those in Toropina et al. (2001). However, here the star rotates in the propeller regime. The main objective of this work is to determine the dependences of spin-down rate of the star on the different variables and to estimate the corresponding time-scale of the spin-down.

Sections 2 and 3 describe the physical situation and simulation model, respectively. In Section 4, we discuss the results of our simulations. In Section 5, we apply our results to magnetars and in Section 6 we discuss possible magnetar candidates. Conclusions are given in Section 7.

2 PHYSICS OF THE 'PROPELLER' REGIME OF A MOVING MAGNETAR

Here, we consider the spin-down of a highly magnetized rotating neutron star or 'magnetar' moving at a velocity v faster than the local sound speed of the ISM; that is, $v > c_s$, where $c_s \approx 10^6\,\mathrm{cm\,s^{-1}}$ for a 10^4 K hydrogen plasma. Theory and simulations of the spin-down for the case of Bondi accretion to a non-moving, rotating magnetized star in the propeller regime were discussed earlier by Romanova et al. (2003). A general discussion and review of theory of the spin-down of moving rotating magnetars is given by Mori & Ruderman (2003).

We first discuss the different length-scales in this problem. Let r_m denote the characteristic size of the star's magnetosphere with the region inside r_m magnetically dominated and corotating with the star at an angular rate Ω_*.

The standoff distance of the bow shock formed by the interaction of the moving ISM with the star's magnetic field is at a distance of the order of

$$r_{st} \equiv \left(\frac{\mu^2}{4\pi\rho v^2}\right)^{1/6} \approx 2.8\times 10^{12}\left(\frac{\mu_{33}^{1/3}}{n^{1/6}v_7^{1/3}}\right)\ \mathrm{cm} \quad (1)$$

from the centre of the star. Here, $\mu_{33} = \mu/10^{33}\ \mathrm{Gcm^3}$ is the star's magnetic moment, n is the number density of the ISM in H/cm^3 and $v_7 \equiv v/(10^7\,\mathrm{cm\,s^{-1}})$. Note that the magnetic field at the star's surface is $B = \mu/R_*^3 = 10^{15}\mu_{33}(10\,\mathrm{km}/R_*)^3$ G, where R_* is the star's radius. We assume that $r_{st} < r_m$.

In the propeller regime, the magnetospheric radius r_m is larger than the corotation radius

$$r_{cr} \equiv \left(GM/\Omega_*^2\right)^{1/3} \approx 1.7\times 10^{10}P_3^{2/3}\,\mathrm{cm}, \quad (2)$$

where P is the rotation period of the star and $P_3 \equiv P/10^3$ s. We assume $M = 1.4\,\mathrm{M_\odot}$ here and subsequently. Consequently, the incoming matter is flung away from the star in the equatorial plane.

A further characteristic length is

$$r_v \equiv v/\Omega_* = 1.5\times 10^9 v_7 P_3\,\mathrm{cm}. \quad (3)$$

This is the distance the star moves in a rotation period divided by 2π. A related length is

$$r_s \equiv c_s/\Omega_*, \quad (4)$$

where c_s is the sound speed in ambient ISM. Other characteristic lengths can be constructed from combinations of equations (1)–(4). For example, the Bondi radius is given by $r_B = r_{cr}^3/r_s^2$ and the Bondi–Hoyle radius by $r_{BH} = r_{cr}^3/r_v^2$.

Additionally, there is a length-scale associated with the magnetic diffusivity, η,

$$r_\eta \equiv (\eta/\Omega_*)^{1/2}. \quad (5)$$

Roughly, r_η is the distance the magnetic field can diffuse in a rotation period of the star. These lengths are expected to be small compared with the lengths (equations 1–4). Note that magnetic diffusivity is much more important in this problem, compared to the viscosity, so that we do not take into account the viscosity in the analysis below.

Note also that we assume the light cylinder radius,

$$r_L = cP/2\pi \approx 4.8\times 10^{12}P_3\,\mathrm{cm}, \quad (6)$$

is larger than the standoff distance r_{st}.

2.1 Torque derived from dimensional analysis

The rate of spin-down of the star is estimated as $\mathrm{d}L/\mathrm{d}t = I\,\mathrm{d}\Omega_*/\mathrm{d}t \approx -4\pi r_m^2 f r_m B_m^2/4\pi$, which is the magnetic torque at the radius r_m, where I is the star's moment of inertia and f is the fraction of the solid angle where this torque acts. We have assumed that $|B_\phi| \approx B_m$ at r_m. Thus

$$\frac{\mathrm{d}L}{\mathrm{d}t} = I\frac{\mathrm{d}\Omega_*}{\mathrm{d}t} \approx -\frac{f\mu^2}{r_m^3}. \quad (7)$$

We take an empirical approach to determine the dependences of the magnetospheric radius r_m on the different physical parameters

$$r_m = r_m(\rho,\ \mu,\ v,\ c_s,\ \Omega_*,\ \eta), \quad (8)$$

as suggested by Mori & Ruderman (2003). We write

$$r_m = (r_{st})^\alpha (r_{cr})^\beta (r_\eta)^\gamma (r_s)^\epsilon (r_v)^s, \quad (9)$$

where $s \equiv 1-\alpha-\beta-\gamma-\epsilon$. Consequently,

$$\frac{\mathrm{d}L}{\mathrm{d}t} \propto -\rho^{\alpha/2}\mu^{2-\alpha}\eta^{-3\gamma/2}c_s^{-3\epsilon}v^{3s-\alpha}\Omega_*^q, \quad (10)$$

where $q = 2\beta + 3\gamma/2 + 3\epsilon + 3s$. In Section 4, we discuss the values of the exponents suggested by our simulations.

2.2 Torque derived from analytical models

There is a wide variety of theories which predict different dependences for the spin-down torque. The dependences are summarized in tables by Davies et al. (1979) and by MR03. For example, from the table in MR03 we see that the power-law dependence on Ω varies strongly, from $n_\Omega = -1$ up to 2; the power-law dependence on μ varies less dramatically from $n_\mu = 2/3$ up to 5/3. The dependence on the star's velocity varies dramatically from $n_v = -5/3$ to 7/3. The dependence on the density of the ISM varies from $n_\rho = 1/6$ to 2/3. The torque obtained from the different models differs by several orders of magnitude. The spin-down time-scales vary correspondingly. One of the reasons for the differences is that in different situations (disc accretion, wind accretion to the non-moving or moving pulsar), the physics of interaction is different. Only a few papers deal with the situation considered in this paper, where the magnetospheric radius is larger than the gravitational capture radius. One consequence of this is that the magnetospheric radius r_m is of the order of the standoff radius r_{st}. Below, we propose a simple physical theory which is closest to our particular problem.

2.3 Torque derived from a simple physical model

Here, we give a simple model for the spin-down of a moving propeller star. We assume that the magnetospheric radius is larger than the accretion radius so that the magnetosphere is an obstacle for the interstellar matter. Matter stops at the standoff distance r_{st} determined from the balance of the ram pressure of the ISM and the

magnetic pressure of the star and is given by equation (1). The mass flow crossing the area $\pi r_{\rm st}^2$ is

$$\dot{M} = \pi r_{\rm st}^2 \rho v.$$

We assume that a fraction $f = k[\eta/(r_{\rm st}v)]^s$ of this mass flux participates in spinning-down of the star, where $Re_{\rm m} = r_{\rm st}v/\eta$ is the magnetic Reynolds number and k and s are constants. The factor f is determined by the penetration of the interstellar plasma into the star's magnetosphere. The larger the penetration the larger is the transfer of angular momentum from the star to the ISM. Noting that $\Omega_* r_{\rm st}^2$ is the specific angular momentum of the matter at a distance $r_{\rm st}$, we obtain

$$\frac{{\rm d}L}{{\rm d}t} = -k\left(\frac{\eta}{r_{\rm st}v}\right)^s \dot{M}\Omega_* r_{\rm st}^2 \approx -k\eta^s \rho^{\frac{(s+2)}{6}} \mu^{\frac{(4-s)}{3}} v^{\frac{-(1+2s)}{3}} \Omega_*.$$

As an illustration, consider $s = 0.3$ which is suggested by our simulations (see Fig. 4d). We then find

$$\frac{{\rm d}L}{{\rm d}t} = -k\eta^{0.3}\rho^{0.4}\mu^{1.2}\Omega_* v^{-0.5}. \quad (11)$$

This model indicates that the torque increases with μ, ρ and Ω_*, but it decreases with increasing velocity v.

2.4 Transition from pulsar to propeller stages

Equating the standoff distance $r_{\rm st}$ to the light cylinder radius $r_{\rm L}$ gives an estimate of the transition from the pulsar stage to the propeller stage,

$$P_{\rm trans} = 5.6 \times 10^2 \left(\frac{\mu_{33}^{1/3}}{n^{1/6} v_7^{1/3}}\right) \ {\rm s}. \quad (12)$$

The propeller stage will end when the corotation radius $r_{\rm cr}$ is larger than the magnetospheric radius $r_{\rm st}$. This occurs for

$$P = 2.1 \times 10^6 \left(\frac{\mu_{33}^{1/2}}{n^{1/4} v_7^{1/2}}\right) \ {\rm s}. \quad (13)$$

Thus, a magnetar with field $B = 10^{15}$ G propagating through the ISM supersonically will be in the propeller regime for rotation periods $560 < P < 2 \times 10^6$ s. Our model applies only for this range.

3 NUMERICAL MODEL

We investigate the interaction of the fast moving rotating magnetized star with the ISM using an axisymmetric, resistive MHD code. The code incorporates the methods of local iterations and flux-corrected transport (Zhukov, Zabrodin & Feodoritova 1993). The flow is described by the resistive MHD equations:

$$\begin{aligned}
\frac{\partial \rho}{\partial t} &+ \nabla\cdot(\rho\, \boldsymbol{v}) = 0,\\
\rho\frac{\partial \boldsymbol{v}}{\partial t} &+ \rho(\boldsymbol{v}\cdot\nabla)\boldsymbol{v} = -\nabla p + \frac{1}{c}\boldsymbol{J}\times\boldsymbol{B} + \boldsymbol{F}^{\rm g},\\
\frac{\partial \boldsymbol{B}}{\partial t} &= \nabla\times(\boldsymbol{v}\times\boldsymbol{B}) + \frac{c^2}{4\pi\sigma}\nabla^2\boldsymbol{B},\\
\frac{\partial(\rho\varepsilon)}{\partial t} &+ \nabla\cdot(\rho\varepsilon\boldsymbol{v}) = -p\nabla\cdot\boldsymbol{v} + \frac{\boldsymbol{J}^2}{\sigma}. \quad (14)
\end{aligned}$$

We assume axisymmetry ($\partial/\partial\phi = 0$), but calculate all three components of velocity and magnetic field $\boldsymbol{v}$ and $\boldsymbol{B}$. The equation of state is taken to be that for an ideal gas, $p = (\gamma - 1)\rho\varepsilon$, with specific heat ratio $\gamma = 5/3$. The equations incorporate Ohm's law $\boldsymbol{J} = \sigma(\boldsymbol{E} + \boldsymbol{v}\times\boldsymbol{B}/c)$, where σ is the electrical conductivity. The associated magnetic diffusivity, $\eta_{\rm m} \equiv c^2/(4\pi\sigma)$, is considered to be a constant within the computational region. In equation (2), the gravitational force, $\boldsymbol{F}^{\rm g} = -GM\rho\boldsymbol{R}/R^3$, is due to the central star.

We use a cylindrical, inertial coordinate system (r, ϕ, z) with the z-axis parallel to the star's dipole moment $\boldsymbol{\mu}$ and rotation axis $\boldsymbol{\Omega}$. The vector potential $\boldsymbol{A}$ is calculated so that $\nabla\cdot\boldsymbol{B} = 0$ at all times. The star rotates with the angular velocity $\boldsymbol{\Omega}_* = \Omega_*\,\hat{\boldsymbol{z}}$. The intrinsic magnetic field of the star is taken to be an aligned dipole, with the vector potential $\boldsymbol{A} = \boldsymbol{\mu}\times\boldsymbol{R}/R^3$.

We measure length in units of the Bondi radius $R_{\rm B} \equiv GM/c_{\rm s}^2$, with $c_{\rm s}$ being the sound speed at infinity, density in units of the density of the ISM ρ and magnetic field strength in units of B_0 which is the field at the pole of the numerical star. The magnetic moment is measured in units of $\mu_0 = B_0 R_{\rm B}^3/2$.

After reduction to dimensionless form, the MHD equations involve dimensionless parameters,

$$\beta \equiv \frac{8\pi P_0}{B_0^2}, \qquad \tilde{\eta}_{\rm m} \equiv \frac{\eta_{\rm m}}{R_{\rm B} v_0} = \frac{1}{Re_{\rm m}}, \quad (15)$$

where $\tilde{\eta}_{\rm m}$ is the dimensionless magnetic diffusivity, $Re_{\rm m}$ is the magnetic Reynolds number and β is the so-called gravimagnetic parameter, which describes the ratio between pressure of the ISM medium and magnetic field at the poles of the 'numerical' star, B_0.

Simulations were done in a cylindrical region ($Z_{\rm min} \leqslant z \leqslant Z_{\rm max}, 0 \leqslant r \leqslant R_{\rm max}$). The numerical star was represented by a small cylindrical box with dimensions $R_* \ll R_{\rm max}$ and $|Z_*| \ll Z_{\rm max}$. A uniform (r, z) grid with $N_R \times N_Z$ cells was used.

Initially, the density $\rho(r, z)$ and the velocity $\boldsymbol{v}(r, z)$ are taken to be constant in the region $\rho(r, z) = \rho$ and $v = v_*$, $v_\phi = 0$. Also, initially the vector potential $\boldsymbol{A}$ was taken to that of a dipole so that $B_\phi = 0$. The vector potential was fixed inside the numerical star and at its surface during the simulations. The star was initialized to be rotating at the rate Ω_*.

The outer boundaries of the computational region were treated as follows. Supersonic inflow with the Mach number $\mathcal{M}$ was specified at the upstream boundary ($z = Z_{\rm min}$, $0 \leqslant r \leqslant R_{\rm max}$). The variables $(\rho, v_r, v_z, \varepsilon)$ are fixed. The inflowing matter is unmagnetized with $\boldsymbol{B} = 0$. At the downstream boundary ($z = Z_{\rm max}, 0 \leqslant r \leqslant R_{\rm max}$) and at the cylindrical boundary ($Z_{\rm min} \leqslant z \leqslant Z_{\rm max}, r = R_{\rm max}$), a free boundary condition was applied, $\partial/\partial\boldsymbol{n} = 0$. Boundary conditions are described in greater detail in T01 and R03.

The size of the computational region for most of the simulations was $R_{\rm max} = 0.9R_{\rm B} = 0.9$, $Z_{\rm min} = -R_{\rm max} = -0.9$, with $Z_{\rm max} = 2R_{\rm max} = 1.8$. The grid $N_R \times N_Z$ was 289×865 in most of cases. The radius of the numerical star was $R_* = 0.025R_{\rm B} = 0.025$ in all cases.

4 RESULTS

We investigated numerically interaction of the rotating magnetar with the ISM and the rate of spinning-down. Simulations were done at a variety of parameters: magnetic moments of the star μ, angular velocities Ω_*, Mach numbers $\mathcal{M}$ and diffusivities $\tilde{\eta}$. In most cases, we varied one parameter in a time, and kept other parameters fixed and corresponding to the 'main' case. In the main case, a star rotates with an angular velocity $\omega_* = \Omega_*/\Omega_{\rm K*} = 0.7$, where $\Omega_{\rm K*} = \sqrt{GM/R_*^3}$ is the Keplerian angular velocity at the surface of the numerical star. We suggest that the numerical star (inner boundary) is much larger than the true radius of the neutron star. The Mach number is $\mathcal{M} = 3$. We take the gravimagnetic parameter $\beta = 10^{-6}$ which corresponds to the dimensionless magnetic moment $\mu = 10^{-7.5}$, and take magnetic diffusivity $\tilde{\eta}_{\rm m} = 10^{-5}$.

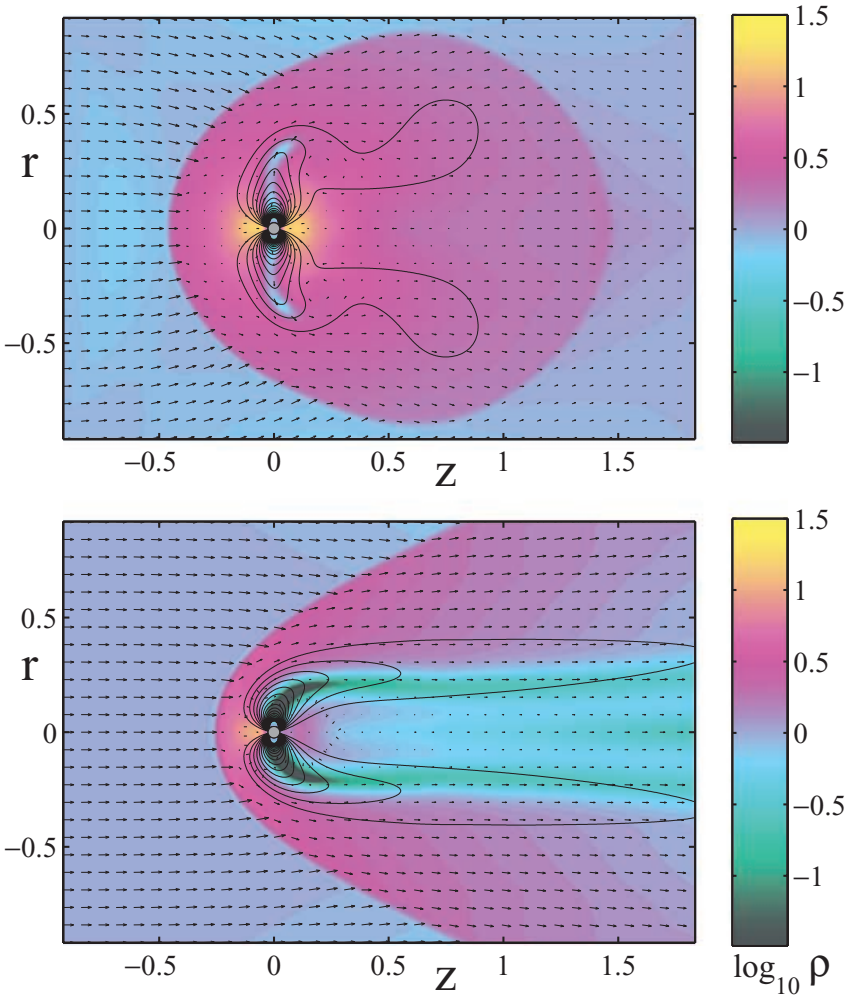

Figure 1. Matter flow around a strongly magnetized star rotating in the propeller regime and propagating through the ISM with the Mach numbers $\mathcal{M} = 1$ (top panel) and $\mathcal{M} = 3$ (bottom panel). Other parameters correspond to the main case. The background represents the logarithm of density and the length of the arrows is proportional to the poloidal velocity. The solid lines are magnetic field lines. The dashed solid line shows the Alfvén surface. Distances are measured in units of the Bondi radius. Time corresponds to 50 rotation periods of the star.

4.1 Dependence of torque on the Mach number

For parameters corresponding to our 'main case', we did simulation runs for the Mach numbers $\mathcal{M} = 1$, 3, 5, 6 and 10, with the ambient sound speed fixed. From these runs, we find that the torque decreases with the Mach number approximately as $\dot{L} \propto -\mathcal{M}^{-0.4}$.

Fig. 1(a) shows that for a Mach number $\mathcal{M} = 1$ the flow is similar to that observed in the case of a *non-moving* propeller (Romanova et al. 2003). Namely, the rapidly rotating magnetosphere pushes matter and magnetic flux outwards in the equatorial plane forming the low-density, rotating torus in the equatorial plane. The gravitational radius is several times larger than the magnetospheric radius so that a significant part of the inflowing matter is gravitationally trapped and accumulates around the star. This is similar to the case of the spherical Bondi accretion to a star in the propeller stage. For $\mathcal{M} = 1$, there is an axial flow of matter downstream from the shock wave. However, the energy density of the inflowing matter $\rho \boldsymbol{v}^2/2$ is smaller than the energy density of the equatorial propeller outflow $\rho \boldsymbol{v}^2/2 + \boldsymbol{B}^2/8\pi$ and this is why the equatorial structure forms.

Fig. 1(b) shows the flow at a larger Mach number $\mathcal{M} = 3$. In this case, the energy density of the ISM matter is larger than the energy density of the equatorial propeller-generated wind, so that the disc structure is bent and pushed to the direction of the tail. This interaction is similar to that observed in the simulations of magnetized supersonic stars in the non-rotating case (Toropina et al. 2001). Namely, the magnetosphere of the star acts as an obstacle for the ISM matter so that a bow shock stands in front of the star and a conical shock wave forms behind it. The standoff distance and the cross-section of the interaction are larger in the propeller case than in the non-rotating case. This is because the rotating equatorial disc of matter and magnetic field generated by the fast rotating magnetosphere. For Mach numbers $\mathcal{M} > 2$–3, this disc structure is pushed by the inflowing matter into a magnetotail behind the star. The maximum rotational velocity of the magnetosphere $v_{\rm prop} = r\Omega_*$ is several times larger than the velocity of the ISM matter, v. In common terminology, the propeller is 'supersonic'. In spite of this, the ISM matter pushes this fast rotating matter together with the magnetic field into the magnetotail. Because of angular momentum conservation, the matter in the magnetotail continues to rotate. In addition, the magnetic field is twisted by the rotating matter. The amount of the twist depends on the parameters. For the parameters of our main case, the twist is $B_\phi/B_{\rm p} \sim 0.1$.

For even larger Mach numbers, $\mathcal{M} = 6$–10, the flow is similar to that observed for $\mathcal{M} = 3$. However, the standoff distance is even

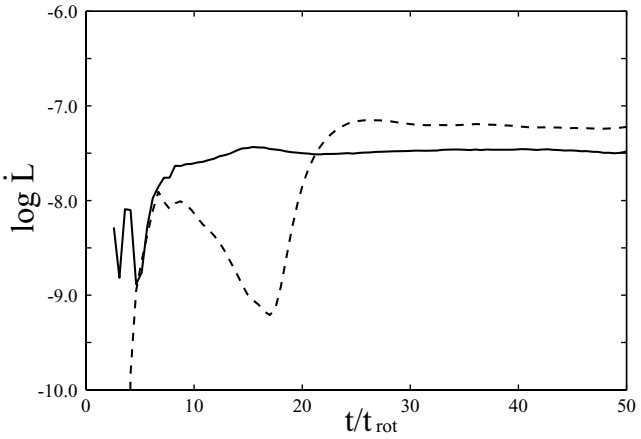

Figure 2. Temporal variation of the total angular momentum flux from the star obtained by integrating over a surface surrounding the star (solid line) and the flux through a surface across the magnetotail at $z = 0.6$ (dotted line).

smaller, because the larger portion of the rotating magnetosphere is pushed into the magnetotail behind the star.

The rotating magnetosphere interacts with the non-rotating matter of the ISM and this leads to the spinning-down of the star. Angular momentum lost by the star flows out from the star. Thus, we calculate the torque on the star by integrating the angular momentum flux density over a surface surrounding the star,

$$\dot{L} = -\int \mathrm{d}\boldsymbol{S} \cdot \left(\rho \boldsymbol{v}_\mathrm{p} r v_\phi - \frac{\boldsymbol{B}_\mathrm{p} r B_\phi}{4\pi} \right).$$

Here, d $\boldsymbol{S}$ is the outward pointing surface area element and the subscript p indicates the poloidal component. We use a cylindrical surface around the star approximately at the Alfvén surface to evaluate this integral. Fig. 2 (solid line) shows temporal variation of this flux. One can see that after a few initial rotations of the star, $\dot{L}$ becomes approximately constant. For comparison, we also calculated angular momentum flux through the magnetotail at the distance $z = 0.6$ from the star. We obtained similar value of the angular momentum flux (see dashed line at Fig. 2) because the angular momentum lost by the star flows into the magnetotail.

Fig. 3 shows distribution of angular momentum flux densities carried by the magnetic field $-\boldsymbol{B}_\mathrm{p} r B_\phi/4\pi$ (top panel) and that carried by the matter $\rho \boldsymbol{v}_\mathrm{p}\ r v_\phi$ (bottom panel). One can see that inside the star's magnetosphere the magnetic field gives the main contribution to the angular momentum flux (see the top panel). After passing the shock wave, the magnetosphere interacts with the non-rotating ISM and transports part of its angular momentum to the matter. This rotating matter propagating to the magnetotail gives the main contribution to the angular momentum flux in the tail (see the bottom panel). The rate of angular momentum loss from the star depends on the efficiency of mixing of the ISM matter with the magnetic field of the magnetosphere.

4.2 Dependence of the torque on other parameters

We performed a number of simulations with different angular velocities of the star Ω_* and different magnetic moments μ. We calculated the total angular momentum loss rate from the star and investigated its dependence on the Ω_* and μ.

Fig. 4(b) shows the total angular momentum loss rate from the star as a function of Ω_*. We find that for the main case (the Mach number $\mathcal{M} = 3$) this dependence is $\dot{L} \propto -\Omega_*^{1.5}$. This dependence is somewhat stronger than that found for a non-moving star where $\dot{L} \propto -\Omega_*^{1.3}$ (Romanova et al. 2003). We expected that at the Mach number $\mathcal{M} = 1$ the torque will have a power between 1.5 and 1.3, however, we obtained the value $q = 1.1$ (see Fig. 4b, rhombus). This may be connected with different physics of interaction at very large and very small Mach numbers.

Fig. 4(c) shows the total angular momentum loss rate from the star as a function of μ. Approximately, $\dot{L} \propto -\mu^{0.6}$. This dependence is similar to that for the case of non-moving star $\dot{L} \propto -\mu^{0.8}$ (Romanova et al. 2003).

We also calculated the dependence of the torque on diffusivity, and obtained $\dot{L} \propto -\eta^{0.3}$. Diffusivity is an important factor which helps to mix non-rotating matter of the ISM with rotating magnetosphere. It is one of the important factors which determines the amount of matter participating in spinning-down.

In addition, we calculated the dependence of the torque on the density of the ISM medium and obtained the dependence $\dot{L} \propto -\rho^{0.8}$.

4.3 Summary of scaling laws

Taking into account all the above dependences, we obtain the summary of scaling laws:

$$\frac{\mathrm{d}L}{\mathrm{d}t} \propto -\rho^{0.8} \mu^{0.6} \eta^{0.3} \mathcal{M}^{-0.4} \Omega_*^{1.5}. \tag{16a}$$

The dependences do not exactly coincide with those derived in the simple physical model (Section 2.3, equation 11), however, the main tendencies do coincide. It is important to note that in both cases the dependence on the Mach number (velocity of the star, v, in the physical model) is *negative*. This is a robust result which was understood analytically and confirmed in simulations.

We also can compare these empirical dependences with scaling laws proposed in Section 2.1. The dependence of $\dot{L}$ on the magnetic moment μ implies that $\alpha \approx 1.4$. The dependence of $\dot{L}$ on the magnetic diffusivity η implies that $\gamma \approx -0.2$. The dependence of $\dot{L}$ on the velocity of the star v or the Mach number $\mathcal{M}$ implies that $\beta + \epsilon \approx -0.8$. The dependence of $\dot{L}$ on the star's rotation rate Ω_* implies that $\beta \approx -2.4$. Thus, equation (10) implies that

$$\frac{\mathrm{d}L}{\mathrm{d}t} \propto -\rho^{0.7} \mu^{0.6} \eta^{0.3} c_\mathrm{s}^{-3\epsilon} v^{-0.4} \Omega_*^{1.5}. \tag{16b}$$

Note that the dependence on density $\rho^{0.7}$ was derived from the scaling analysis and it is very close to that obtained from the numerical simulations.

The dependences we find of $\dot{L}$ on μ, v and Ω are not compatible with equation (4) of Mori & Ruderman (2003) because different approaches were used.

5 SPINNING-DOWN OF MAGNETARS

Let us estimate spinning down of magnetars in real, dimensional units. We take as a base our main dimensionless parameters: angular velocity $\Omega/\Omega_{\mathrm{K}*} = 0.7$, the Mach number $\mathcal{M} = 3$, gravimagnetic parameter $\beta = 10^{-6}$ and magnetic diffusivity $\tilde{\eta}_\mathrm{m} = 10^{-5}$.

Let us consider a neutron star with mass $M = 1.4\ \mathrm{M}_\odot = 2.8 \times 10^{33}$ g and radius $R_\mathrm{NS} = 10^6$ cm. The density of the ambient interstellar matter is taken to be $\rho = 1.7 \times 10^{-24}\ \mathrm{g\,cm^{-3}}$ ($n = 1\ \mathrm{cm^{-3}}$). The sound speed in the ISM, $c_\mathrm{s} = 30\ \mathrm{km\ s^{-1}}$ and a star moves in the ISM with velocity $v = 3\, c_\mathrm{s} = 90\ \mathrm{km\ s^{-1}}$.

Using the definitions $\beta = 8\pi p/B_0^2$ and $p = \rho c_\mathrm{s}^2/\gamma$, we obtain the magnetic field at the surface of the 'numerical' star $B_0 = (8\pi/\gamma\beta)^{1/2} \rho^{1/2} c_\mathrm{s} \approx 0.15\, n_1 c_{30}$ G.

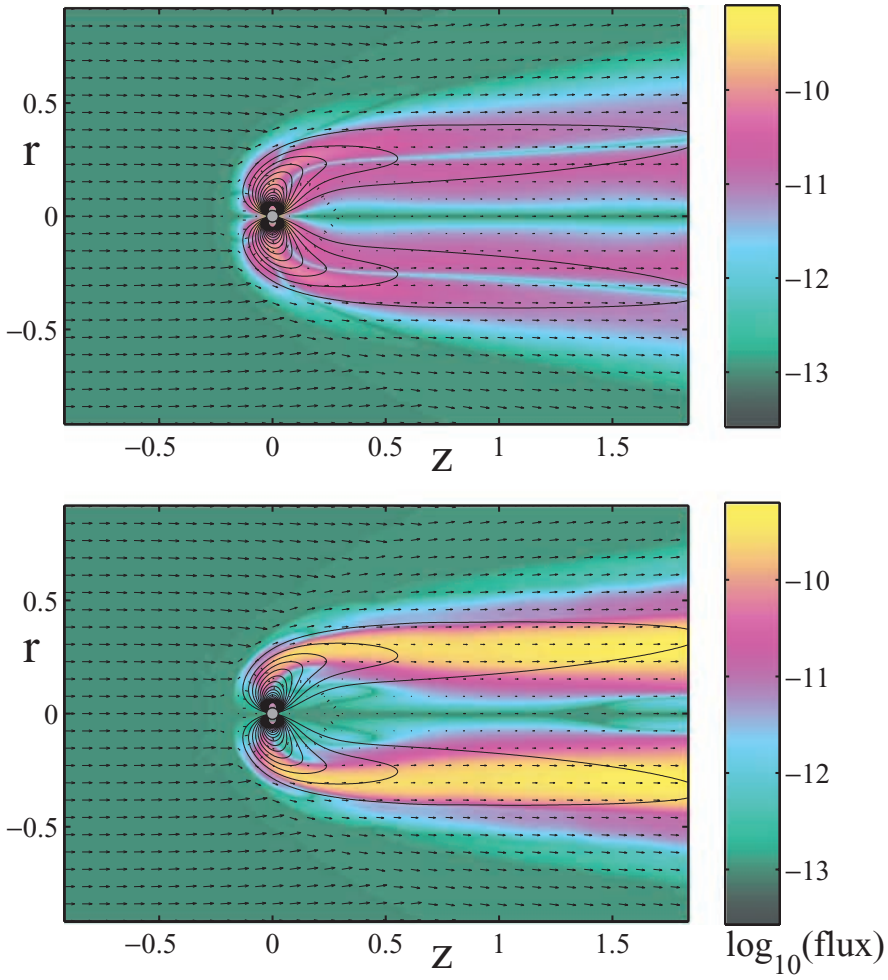

Figure 3. Distribution of the angular momentum fluxes in the magnetotail for our main case. The colour background shows the specific angular momentum carried by the magnetic field (top panel) and by the matter (bottom panel). The solid lines are magnetic field lines.

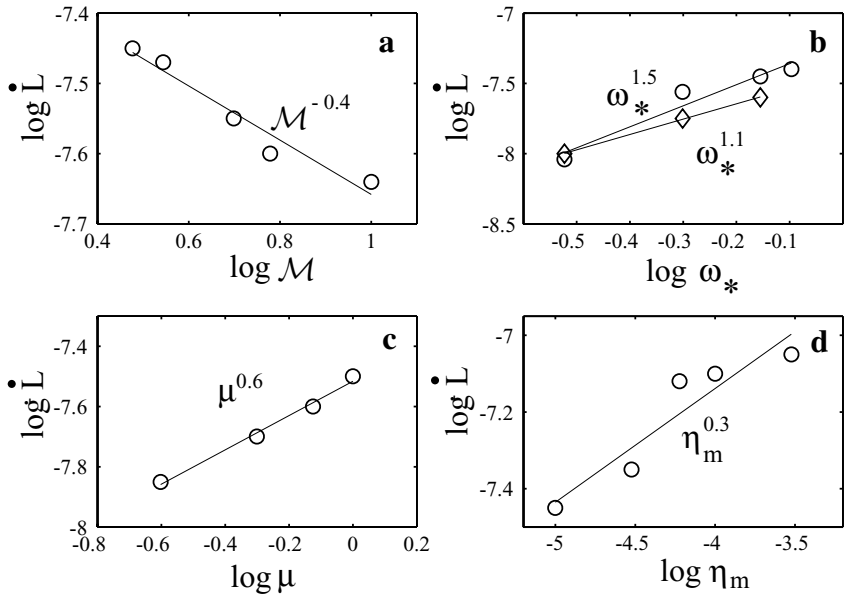

Figure 4. Dependence of the angular momentum flux on different parameters: (a) the Mach number $\mathcal{M}$, (b) the angular velocity of the star $\omega_* \equiv \Omega_*/\Omega_K$, (c) the magnetic moment μ and (d) the magnetic diffusivity $\tilde{\eta}_m$.

We use the Bondi radius as a length-scale. This radius is

$R_{\rm B} = GM_*/c_{\rm s}^2 \approx 2.1 \times 10^{13} c_{30}^{-2}$ cm.

Recall that the size of the numerical star is $R_* = 0.025\,R_{\rm B} \approx 5.2 \times 10^{11} c_{30}^{-2}$ cm in all simulations. Thus, the magnetic moment of the numerical star is $\mu = B_0\, r_*^3/2 \approx 1 \times 10^{33} n_1 c_{30}^{-5}$ G cm^3. Note that this is of the order of the magnetic moment of a real neutron star with surface field $B_{\rm NS} = 10^{15}$ G and radius $R_{\rm NS} = 10^6$ cm. Therefore, we can suggest that a real neutron star is hidden inside the numerical star. The neutron star with so strong magnetic field is considered as a magnetar.

The numerical star in our main case rotates with angular velocity $\Omega_* = 0.7\,\Omega_{\rm K*} = 2.5 \times 10^{-5}$ s^{-1} and this corresponds to a period of $P_* = 2\pi/\Omega_* \approx 2.5 \times 10^5$ s.

For these parameters, the corotation radius, $R_{\rm cor} = (GM/{\Omega_*}^2)^{1/3} = R_*/{\omega_*}^{2/3} \approx 1.3R_*$, is appreciably less than $R_{\rm m} \approx 5R_*$. The light cylinder radius, $R_{\rm L} = cP/2\,\pi = 1.17 \times 10^{15} P_5$ cm, is greater than the radius of magnetosphere taken from simulations $R_{\rm m} \approx 2.5 \times 10^{12} c_{30}^{-2}$ cm. Therefore, this case $R_{\rm cor} \leqslant R_{\rm m} \leqslant R_{\rm L}$ corresponds to the propeller regime.

Therefore, our simulations model an isolated magnetar which spins down by the propeller effect.

Now, we can estimate a time of spin-down due to the propeller torque using equation (9). An angular momentum of a star is equal to $L_* = I_*\Omega_*$, where $I_* = 2/5\,M_*R_*^2$ – moment of inertia for sphere. Taking $I_* \approx 10^{45}$ g cm^2 and $\Omega_* = 2\,\pi/P_*$, we obtain $L_* = 2\,\pi I_*/P_* \approx 3 \times 10^{40} P_5^{-1}$ g cm^{-2} s^{-1}.

The angular momentum loss rate $\dot{L} = \tilde{\dot{L}}\dot{L_0}$, where for typical simulation run we find $\tilde{\dot{L}} \approx 10^{-7}$. Taking into account dimensional parameter $\dot{L_0} \approx -3 \times 10^{36} n_1 c_{30}^{-4}$ g (cm s^{-1})^2, we obtain $\dot{L} \approx -3 \times 10^{29} n_1 c_{30}^{-4}$ g (cm s^{-1})^2.

In reality, $\dot{L}$ is not a constant and depends on many parameters – velocity of the star, angular velocity and magnetic field of the neutron star. We performed a number of simulations with different angular velocities Ω_* and different magnetic moments μ of the star and find dependences: $\dot{L} \propto \Omega_*^3 \mu^{0.6} \mathcal{M}^{-0.4}$, or $\dot{L} \propto P_*^{-1.5} \mu^{0.6} \mathcal{M}^{-0.4}$. Thus,

$$\dot{L} \approx 3 \times 10^{29} n_1 c_{30}^{-4} B_{15}^{0.6} P_5^{-1.5} \mathcal{M}_3^{-0.4} \text{ g (cm s}^{-1})^2. \quad (17a)$$

Thus, the characteristic spin-down time is

$$T = L_*/|\dot{L}| \approx 10^4\, n_1^{-1} c_{30}^4 B_{15}^{-0.6} P_5^{0.5} \mathcal{M}_3^{0.4} \text{ yr}. \quad (17b)$$

Now, we can estimate the time-scale of evolution at the propeller stage. For periods $P_* = 10^3$ s, which correspond to the beginning of the propeller stage, the evolution scale will be $\Delta T = 10^3$ yr, while at period $P_* = 10^6$ s corresponding to the end of the propeller stage $T = 3 \times 10^4$ yr. Thus we see that magnetars are expected to spin down very fast at the propeller stage. This time-scale, however, may be much larger if diffusivity is very small.

5.1 Restrictions of the model

The axisymmetric resistive MHD numerical code used in this paper is a robust and has been checked at a number of tests and also it has been used for the solution of similar, but somewhat simpler, problems, such as Bondi accretion to a non-moving star, wind accretion to a moving magnetized non-rotating star and others. This paper is a logical continuation of the series of simulations with increased complexity. The bow shock which forms in our simulations is similar to the one obtained in simulations of the Earth's magnetosphere interacting with the solar wind (e.g. Gombosi, Powell & van Leer 1999) and simulations of the pulsar wind interacting with the magnetosphere of the companion neutron star (Arons et al. 2005).

However, there is one factor which is important and basically is not known, this is diffusivity. The role of diffusivity was underestimated in the analytical papers on propellers, however, it is very important for mixing of the incoming matter to the magnetic field of the magnetosphere. In our model, we took some value of diffusivity such that a part of the incoming matter diffuses through the field lines and takes part in the spinning-down of the star. However, if the diffusivity will be much smaller, then the time-scale presented by formulae (17b) will increase.

6 DISCUSSION OF POSSIBLE MAGNETAR CANDIDATES

It is not clear whether we can observe old, slowly rotating magnetars. One of the unknown aspects is that we do not know whether magnetic energy will continue to release, and at which rate, and what is the expected spectrum of such radiation. The theory of radiation from relatively fast rotating magnetars has recently been developed (e.g. Beloborodov & Thompson 2006), which predicts radiation from the whole magnetosphere mostly in the X-ray. However, we do not know what would be the luminosity and spectrum of much slower rotating magnetars with periods $P < 10^3$ s and thus it is not clear how to find them, even if many of them survive. This is an obstacle in searching the old magnetars even with the best modern instruments. There are, however, candidates for magnetars: SGRs and anomalous X-ray pulsars (AXPs) and also the INS candidate RX J1856.5−3754.

6.1 Clustering of periods of SGRs and AXPs

One of amazing properties of SGRs and AXPs, which are strong candidates for magnetars, is the clustering of periods around 6–12 s. This is still a stage when the light cylinder is smaller than the magnetospheric radius, and the processes at the light cylinder may be responsible for the spin-down. The estimated age of these objects is around 10^3–10^4 yr which is evidence of their fast spinning down at this stage. An analysis of possible evolution of periods has shown that after $P > 10$ s, either these objects should spin down much faster or the magnetic field should decay very fast (Psaltis & Miller 2002; see also Colpi, Geppert & Page 2000). The spinning-down at this stage has not been investigated yet. Recent relativistic 3D numerical simulations of aligned and misaligned rotators and further modelling in this direction may help to understand what is the expected spinning-down rate at the pulsar-type stages (Spitkovsky 2004, 2006). Unfortunately, we cannot extrapolate formulae (17b) to much shorter periods, $P \sim 10$ s, because our results are only relevant to the propeller stage with $P > 10^3$ s. Our simulations show, that propeller mechanism is very efficient in spinning-down of magnetars. However, we should remember that there is a big uncertainty in the results of simulations: we do not know, which part of the ISM matter from the cross-section $\sigma = \pi r_{\rm st}^2$ will participate in the spinning-down of the star. This greatly depends on the diffusivity, which is not known. In spite of that, it is important to know the dependences of the torque on different parameters. Therefore, our model cannot explain the clustering, however, if a magnetars with period $P > 10^3$ s will be discovered in the future, then these formulae will describe the subsequent evolution.

6.2 INS candidate RX J1856.5−3754

Of the small number of INS candidates, the object RX J1856.5−3754 is special because it has a $H\alpha$ nebula with the shape of a shock wave (van Kerkwijk & Kulkarni 2001). The origin of this

nebula and the INS candidate is not yet known. One possibility is that it is a misaligned pulsar with magnetic field $B \sim 10^{12}$–10^{13} G and period $P \sim 1$ s. Then the nebulae may be a shock wave which appears as a result of the interaction of the relativistic wind of the pulsar with the ISM (e.g. Romanova et al. 2001; van Kerkwijk & Kulkarni 2001; Braje & Romani 2002; Romanova, Chulsky & Lovelace 2005a). A weak part of this model is the lack of pulsations. The X-ray pulsed fraction is <1.3 per cent (Burwitz et al. 2003). Another idea is that this is an old neutron star which had a recent accretion event and is slowly cooling down. Then the $H\alpha$ nebulae may be connected with the ionization by the ISM (van Kerkwijk & Kulkarni 2001).

Another possible idea is that RX J1856.5−3754 is a relatively old, slowly rotating magnetar (Romanova et al. 2001) which spun-down rapidly during its propeller stage (Mori & Ruderman 2003). This model may explain the lack of pulsations. However, there is no simple explanation of the $H\alpha$ nebulae. In spite of the large cross-section of the bow shock, the energy of the ISM released at the shock $\dot{E}_{\rm shock} \approx 0.5\rho v^3 \pi r_{\rm m}^2 \approx 5\times10^{23} n^{2/3} v_7^{7/3} B_{15}^{2/3}$ erg s^{-1} is much smaller than that of the $H\alpha$ nebulae. Also, reconnection in the magnetotail (Toropina et al. 2001) gives insufficient power. An additional heating mechanism of the star or magnetosphere is necessary to explain the $H\alpha$ nebulae. Heating of the star due to accretion from the ISM is excluded because very little matter accretes to a strongly magnetized star owing to the very narrow accretion columns (Toropina et al. 2003). There is the possibility of heating of the star by the release of the magnetic energy (e.g. Beloborodov & Thompson 2006). However, the magnetic heating of slowly rotating magnetars has not been investigated. Thus the powering the $H\alpha$ nebulae is uncertain but not ruled out.

7 CONCLUSIONS

Using axisymmetric MHD simulations, we have studied the supersonic propagation through the ISM of magnetars in the propeller stage. We have done many simulation runs for the purpose of determining the angular momentum loss rate of the star due to the interaction of its magnetosphere with the shocked ISM. We conclude that the interaction may be highly effective in spinning-down magnetars. A star with magnetic field $B \sim 10^{13}$–10^{15} G is expected to spin down in $\Delta T \sim 10^4$–10^5 yr. This time may be longer if the ISM material does not efficiently interact with the external regions of the magnetar's magnetosphere. Therefore, after relatively short stages of pulsar and propeller activity, a magnetar becomes a very slowly rotating object, with a period $P > 10^5$–10^6 s, which is much longer than the periods expected for ordinary pulsars. This may be a reason why the number of SGRs, which are candidate magnetars, is so small. We should note, however, that the rate of spinning-down depends on the magnetic diffusivity which is not known. At lower diffusivity, the rate of spinning-down will be lower. The INS candidate RX J1856.5−3754 may be an example of a slowly rotating magnetar. However, this model does not explain the $H\alpha$ nebulae. An ordinary misaligned pulsar explains the different features more easily, excluding the fact that no periodic fluctuations were observed from this object.

ACKNOWLEDGMENTS

This work was supported in part by NASA grants NAG5-13220, NAG5-13060, by NSF grant AST-0507760 and by Russian programme 'Astronomy'. We thank the anonymous referee for valuable suggestions, Dr V. V. Savelyev for the development of the original version of the MHD code used in this work and Dr Yuriy Toropin for discussions.

REFERENCES

Arons J., Backer D. C., Spitkovsky A., Kaspi V. M., 2005, in Rasio F. A., Stairs I. H., eds, ASP Conf. Ser. Vol. 328, Binary Radio Pulsars. Astron. Soc. Pac., San Francisco, p. 95
Beloborodov A. M., Thompson C., 2006, ApJ, in press (astro-ph/0602417)
Braje T. M., Romani R. W., 2002, ApJ, 580, 1043
Burwitz V., Haberl F., Neuhäuser R., Predehl P., Trümper J., Zavlin V. E., 2003, A&A, 399, 1109
Colpi M., Geppert U., Page D., 2000, ApJ, 529, L29
Davidson K., Ostriker J. P., 1973, ApJ, 179, 585
Davies R. E., Pringle J. E., 1981, MNRAS, 196, 209
Davies R. E., Fabian A. C., Pringle J. E., 1979, MNRAS, 186, 779
Duncan R. C., Thompson C., 1992, ApJ, 392, L9
Gombosi T. I., Powell K. G., van Leer B., 1999, J. Geophys. Res., 105, 13141
Harding A. K., Leventhal M., 1992, Nat, 357, 388
Hurley K. et al., 1999, Nat, 397, 41
Ikhsanov N. R., 2002, A&A, 381, L61
Illarionov A. F., Sunyaev R. A., 1975, A&A, 39, 185
Kouveliotou C. et al., 1994, Nat, 368, 125
Kouveliotou C. et al., 1998, Nat, 393, 235
Kouveliotou C. et al., 1999, ApJ, 510, L115
Kulkarni S. R., Frail D. A., 1993, Nat, 365, 33
Lipunov V. M., 1992, Astrophysics of Neutron Stars. Springer-Verlag, Berlin
Lovelace R. V. E., Romanova M. M., Bisnovatyi-Kogan G. S., 1999, ApJ, 514, 368
Mori K., Ruderman M. A., 2003, ApJ, 592, L75
Psaltis D., Miller M. C., 2002, ApJ, 578, 325
Rappaport S. A., Fregeau J. M., Spruit H., 2004, ApJ, 606, 436
Romanova M. M., Toropina O. D., Toropin Yu. M., Lovelace R. V. E., 2001, in Wheeler J. C., Martel H., eds, AIP Conf. Proc. Vol. 586, Texas Symposium on Relativistic Astrophysics. Am. Inst. Phys., New York, p. 519
Romanova M. M., Toropina O. D., Toropin Yu. M., Lovelace R. V. E., 2003, ApJ, 588, 400
Romanova M. M., Ustyugova G. V., Koldoba A. V., Lovelace R. V. E., 2004, ApJ, 616, L151
Romanova M. M., Chulsky G. A., Lovelace R. V. E., 2005a, ApJ, 630, 1020
Romanova M. M., Ustyugova G. V., Koldoba A. V., Lovelace R. V. E., 2005b, ApJ, 635, L165
Rutledge R. E., 2001, ApJ, 553, 796
Shvartsman V. F., 1970, Radiofizika, 13, 1852
Spitkovsky A., 2004, in Gaensler F. C., Gaensler B. M., eds, IAU Symp. Vol. 218, Young Neutron Stars and Their Environments. Astron. Soc. Pac., San Francisco, p. 357
Spitkovsky A., 2006, ApJL, preprint (astro-ph/0603147)
Thompson C., Duncan R. C., 1995, MNRAS, 275, 255
Toropin Yu. M., Toropina O. D., Savelyev V. V., Romanova M. M., Chechetkin V. M., Lovelace R. V. E., 1999, ApJ, 517, 906
Toropina O. D., Romanova M. M., Toropin Yu. M., Lovelace R. V. E., 2001, ApJ, 561, 964
Toropina O. D., Romanova M. M., Toropin Yu. M., Lovelace R. V. E., 2003, ApJ, 593, 472
Ustyugova G. V., Koldoba A. V., Romanova M. M., Lovelace R. V. E., 2006, ApJ, in press
van Kerkwijk M. H., Kulkarni S. R., 2001, A&A, 380, 221
Vasist G., Gotthelf E. V., 1997, ApJ, 486, L129
Wang Y.-M., Robertson J. A., 1985, A&A 151, 361
Zhukov V. T., Zabrodin A. V., Feodoritova O. B., 1993, Comput. Maths. Math. Phys., 33, 1099

This paper has been typeset from a TEX/LATEX file prepared by the author.